A Finite-Difference Frequency-Domain Method that Introduces Condensed Nodes and Image Principle

Messan M. Afande, Ke Wu, *Senior Member, IEEE*, Marcel Giroux, and Renato G. Bosisio, *Senior Member, IEEE*

***Abstract*—A new finite-difference frequency-domain formulation is derived from the integral form of Maxwell's equations. Condensed cubic *cell* and 3D node are proposed thereby eliminating field discontinuity in the discrete space domain. Deterministic solutions using a reduced 2D condensed *node* are also presented for standard eigenvalue problems. This method is free from spurious modes by reinforcing electric and magnetic flux conservation among neighboring *cells*. An image concept is introduced to model field boundaries. Numerical results are presented for the complex propagation constant to demonstrate convergence behavior and accuracy of the proposed approach. Modal field profiles of various guided modes are shown for dielectric waveguides.**

I. Introduction

WAVEGUIDING structures have been always essential in microwave and optical components as well as power transfer for heating processes. Accurate analyses of these complex structures usually require field-theoretical and numerical methods in either frequency or time domain [1].

The finite-difference time-domain method (FDTD) [2]–[8], based on the differential form of Maxwell's equations in time domain, has been intensively used to study various types of waveguiding structures. Also, the TLM method [9]–[12] has been developed in both time and frequency domains. Time-domain methods are implemented in an iterative process following the time evolution, initiated via an excitation vector.

Frequency-domain analysis remains attractive due to the fact that boundary conditions are easily handled accurately, and accurate hybrid mode information can be determined without resort to expensive calculations. Nevertheless, some frequency-domain methods such as mode-matching method [13] and method of lines [20] suffer from an iterative search for roots of the characteristic determinant. The application of these approaches requires some degree of symmetry or regularity of structure. The finite-difference frequency-domain (FDFD) method, being simple in mesh generation, has been developed in various forms including Maxwell's integral equations [14]–[19] for deterministic solutions.

Previous works on the FDTD method [2]–[7] and the FDFD method [19] are based on Yee's *cell* (Fig. 1(a)) characterized by spatially separated six field components. This artificial space-domain field discontinuity may lead to errors at boundaries and interfaces. This may also affect numerical accuracy and causes difficulty in handling multilayer structure in which the thickness ratio could be significant. To our knowledge, there is no report of a condensed finite-difference *node* derived directly in frequency domain.

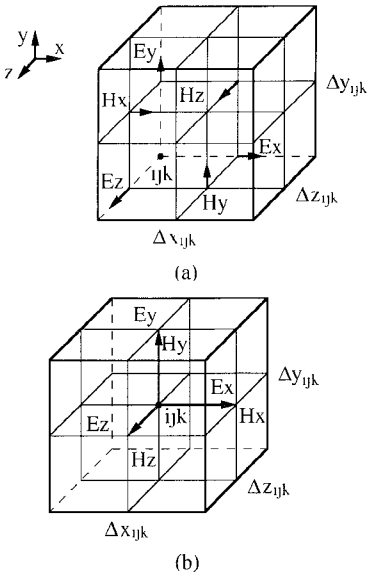

Fig. 1. (a) Yee's *cell*. (b) Condensed *cell*.

In this work, unified 3D and 2D condensed *nodes* are derived from the integral form of Maxwell's equations. A condensed *cell* is considered leading to a better representation of field parameters such as Poynting vector. Electric and magnetic flux conservation between neighboring *cells* are imposed to eliminate spurious modes. In contrast to the conventional way in handling boundary conditions, an image concept is proposed to model boundaries and is successfully used in this work. In addition, this concept leads to the avoidance of dealing directly with edge singularities since field components are not considered on the boundaries. The duality principle can be easily applied to deduce directly E field condensed *node*'s expressions by knowing those of H field condensed *node*, and *vice versa*. An eigenvalue problem is then derived by expressing the interaction between all *nodes* involving the whole structure and the boundaries. Propagation characteristics and modal field profiles are obtained deterministically. Numerical results are presented, thus demonstrating the efficiency of the proposed condensed *node*.

Manuscript received April 11, 1994; revised July 22, 1994.

The authors are with Groupe de Recherches Avancées en Microondes et en Électronique Spatiale, (POLY-GRAMES), Dépt. de Génie Électrique et de Génie Informatique, École Polytechnique, Montréal, Québec, Canada H3C-3A7.

IEEE Log Number 9408566.

0018–9480/95$04.00 © 1995 IEEE

II. THEORY

The integral form of Maxwell's equations (1a)–(1d) in source-free region is considered. The permittivity ε and the permeability μ are complex to account for electric and magnetic dynamic losses as well as electric static losses.

$$\oint_c \vec{E}\cdot d\vec{l} = -\iint_s j\omega\mu\vec{H}\cdot d\vec{s} \tag{1a}$$

$$\oint_c \vec{H}\cdot d\vec{l} = \iint_s j\omega\varepsilon\vec{E}\cdot d\vec{s} \tag{1b}$$

$$\oint_s \varepsilon\vec{E}\cdot d\vec{s} = 0 \tag{1c}$$

$$\oint_s \mu\vec{H}\cdot d\vec{s} = 0 \tag{1d}$$

with

$$\varepsilon = \varepsilon_0\left[\varepsilon' - j\varepsilon'' + \left(\frac{\sigma}{j\omega\varepsilon_0}\right)\right] = \varepsilon_0\varepsilon_r$$
$$\mu = \mu_0(\mu' - j\mu'').$$

The condensed *cell* (Fig. 1(b)), associated with a discrete point ijk, is characterized by the six field components (E_{xijk}, $E_{yijk}, E_{zijk}, H_{xijk}, H_{yijk}, H_{zijk}$), the medium constitutive parameters ($\varepsilon_{rijk}, \mu_{rijk}$) and the mesh grid ($\Delta x_{ijk}$, Δy_{ijk}, Δz_{ijk}).

The condensed *node* is derived in two steps. At first, relations (1a) and (1b) are used to express the field interaction between the condensed *cell* at point ijk and its neighboring *cells*. The discretization scheme is shown in Fig. 2 for $E_{x\imath\jmath k}$ field component at discrete point ijk; discretization scheme for H_{xijk} field component is directly deduced from Fig. 2 by substituting E and H with H and E, respectively. In the following, similar schemes for other field components can be simply deduced by performing an appropriate rotation of the principal axis. To improve the accuracy of the proposed algorithm, a discretization scheme similar to the central difference is used by extending the tangential electric or magnetic field and the normal electric or magnetic flux density to the immediate interconnected *cells*. This is done by applying continuity conditions of the tangential electric or magnetic field and the normal electric or magnetic flux density at a source free interface. Six coupled equations are then obtained in matrix form as follows:

$$\begin{aligned} &-j\omega\mu_0[CH]_{ijk}\vec{H}_{ijk} \\ &\quad = [EIM]_{(i-1)jk}\vec{E}_{(i-1)jk} + [EIP]_{(\imath+1)\jmath k}\vec{E}_{(i+1)jk} \\ &\qquad + [EJM]_{i(\jmath-1)k}\vec{E}_{i(\jmath-1)k}[EJP]_{i(j+1)k}\vec{E}_{i(j+1)k} \\ &\qquad + [EKM]_{ij(k-1)}\vec{E}_{ij(k-1)} + [EKP]_{ij(k+1)}\vec{E}_{ij(k+1)} \end{aligned} \tag{2a}$$

$$\begin{aligned} &j\omega\varepsilon_0[CE]_{ijk}\vec{E}_{ijk} \\ &\quad = [HIM]_{(i-1)jk}\vec{H}_{(\imath-1)jk} + [HIP]_{(i+1)jk}\vec{H}_{(i+1)jk} \\ &\qquad + [HJM]_{i(\jmath-1)k}\vec{H}_{i(\jmath-1)k}[HJP]_{\imath(j+1)k}\vec{H}_{\imath(j+1)k} \\ &\qquad + [HKM]_{ij(k-1)}\vec{H}_{ij(k-1)} + [HKP]_{\imath\jmath(k+1)}\vec{H}_{\imath\jmath(k+1)} \end{aligned} \tag{2b}$$

in which

$$\vec{E} = \begin{bmatrix} E_x \\ E_y \\ E_z \end{bmatrix} \quad \vec{H} = \begin{bmatrix} H_x \\ H_y \\ H_z \end{bmatrix}$$

$$[CH]_{\imath\jmath k} = \begin{bmatrix} CH_x & 0 & 0 \\ 0 & CH_y & 0 \\ 0 & 0 & CH_z \end{bmatrix}_{\imath\jmath k}$$

$$[CE]_{ijk} = \begin{bmatrix} CE_x & 0 & 0 \\ 0 & CE_y & 0 \\ 0 & 0 & CE_z \end{bmatrix}_{\imath\jmath k}$$

$$[EIM]_{(\imath-1)jk} = \begin{bmatrix} 0 & 0 & 0 \\ 0 & 0 & RCE_{yz} \\ 0 & -RCE_{zy} & 0 \end{bmatrix}_{(i-1)\jmath k}$$

$$[EIP]_{(\imath+1)\jmath k} = \begin{bmatrix} 0 & 0 & 0 \\ 0 & 0 & -RCE_{yz} \\ 0 & RCE_{zy} & 0 \end{bmatrix}_{(i+1)\jmath k}$$

$$[EJM]_{i(j-1)k} = \begin{bmatrix} 0 & 0 & -RCE_{xz} \\ 0 & 0 & 0 \\ RCE_{zx} & 0 & 0 \end{bmatrix}_{i(j-1)k}$$

$$[EJP]_{i(j+1)k} = \begin{bmatrix} 0 & 0 & RCE_{xz} \\ 0 & 0 & 0 \\ -RCE_{zx} & 0 & 0 \end{bmatrix}_{i(\jmath+1)k}$$

$$[EKM]_{ij(k-1)} = \begin{bmatrix} 0 & RCE_{xy} & 0 \\ -RCE_{yx} & 0 & 0 \\ 0 & 0 & 0 \end{bmatrix}_{ij(k-1)}$$

$$[EKP]_{\imath\jmath(k+1)} = \begin{bmatrix} 0 & -RCE_{xy} & 0 \\ RCE_{yx} & 0 & 0 \\ 0 & 0 & 0 \end{bmatrix}_{ij(k+1)}$$

Upon the duality principle, the matrices in (2b) can be deduced by replacing E with H. In these characteristic matrices

$$\begin{aligned} CE_{xijk} &= \Delta y_{ijk}\Delta z_{ijk}\varepsilon_{rijk} \\ &\quad + (1/2)[\Delta y_{i(j-1)k}\Delta z_{i(j-1)k}\varepsilon_{ri(j-1)k} \\ &\quad + \Delta y_{i(\jmath+1)k}\Delta z_{i(\jmath+1)k}\varepsilon_{ri(j+1)k} \\ &\quad + \Delta y_{\imath\jmath(k-1)}\Delta z_{\imath\jmath(k-1)}\varepsilon_{r\imath\jmath(k-1)} \\ &\quad + \Delta y_{\imath\jmath(k+1)}\Delta z_{\imath\jmath(k+1)}\varepsilon_{r\imath\jmath(k+1)}] \\ &\quad + (1/4)[\Delta y_{i(\jmath-1)(k-1)} \\ &\quad \times \Delta z_{\imath(j-1)(k-1)}\varepsilon_{ri(j-1)(k-1)} \\ &\quad + \Delta y_{\imath(j-1)(k+1)}\Delta z_{\imath(j-1)(k+1)}\varepsilon_{r\imath(j-1)(k+1)} \\ &\quad + \Delta y_{\imath(j+1)(k-1)}\Delta z_{i(j+1)(k-1)}\varepsilon_{ri(j+1)(k-1)} \\ &\quad + \Delta y_{i(j+1)(k+1)}\Delta z_{i(j+1)(k+1)}\varepsilon_{ri(j+1)(k+1)}] \end{aligned}$$

$$\begin{aligned} RCE_{xz\imath\jmath k} &= \Delta z_{ijk} + (1/2)[\Delta z_{ij(k-1)}(\varepsilon_{r\imath\jmath k}/\varepsilon_{rij(k-1)}) \\ &\quad + \Delta z_{ij(k+1)}(\varepsilon_{rijk}/\varepsilon_{rij(k+1)})] \end{aligned}$$

$$\begin{aligned} RCE_{yxijk} &= \Delta x_{ijk} + (1/2)[\Delta x_{(i-1)jk}(\varepsilon_{rijk}/\varepsilon_{r(i-1)jk}) \\ &\quad + \Delta x_{(i+1)jk}(\varepsilon_{rijk}/\varepsilon_{r(i+1)jk})] \end{aligned}$$

$$\begin{aligned} RCE_{zy\imath\jmath k} &= \Delta y_{ijk} + (1/2)[\Delta y_{i(j-1)k}(\varepsilon_{r\imath\jmath k}/\varepsilon_{r\imath(j-1)k}) \\ &\quad + \Delta y_{i(j+1)k}(\varepsilon_{rijk}/\varepsilon_{ri(j+1)k})] \end{aligned}$$

$$RCE_{zxijk} = RCE_{yx\imath jk}, \quad RCE_{xyijk} = RCE_{zy\imath jk},$$
$$RCE_{yzijk} = RCE_{xzijk}.$$

Due to the symmetry of formulation, coefficients $CE_{y\imath jk}$

and $CE_{z\imath jk}$ can be deduced from the expression of $CE_{x\imath jk}$ by a simple rotation of the principal axis x, y, and z. For example, $CE_{y\imath jk}$ is obtained by replacing Δy, Δz with Δz, Δx, respectively, and modifying adequately the corresponding subscripts. Coefficients $CH_{x\imath jk}$, $CH_{y\imath jk}$, and $CH_{z\imath jk}$ can also be deduced from $CE_{x\imath jk}$, CE_{yijk}, and CE_{zijk} by substituting ε_r by μ_r. Finally, RCH coefficients can be obtained by interchanging ε_r with μ_r in the RCE coefficients. Only the H-field condensed *node* procedure will be exposed since the duality principle can be easily applied. To obtain a decoupled expression described by (3) for H-field components, (2b) is used to eliminate E-field components in (2a) which becomes

$$\begin{aligned}
&[M]_{\imath jk}\vec{H}_{\imath jk} + [MI]_{(\imath-2)jk}\vec{H}_{(\imath-2)jk} + [MI]_{(\imath+2)jk}\vec{H}_{(\imath+2)jk} \\
&\quad + [MJ]_{\imath(j-2)k}\vec{H}_{i(j-2)k} + [MJ]_{\imath(j+2)k}\vec{H}_{i(j+2)k} \\
&\quad + [MK]_{ij(k-2)}\vec{H}_{\imath j(k-2)} + [MK]_{\imath j(k+2)}\vec{H}_{\imath j(k+2)} \\
&\quad + [MIJ]_{(\imath-1)(j-1)k}\vec{H}_{(\imath-1)(j-1)k} \\
&\quad + [MIJ]_{(\imath-1)(j+1)k}\vec{H}_{(\imath-1)(j+1)k} \\
&\quad + [MIJ]_{(i+1)(j-1)k}\vec{H}_{(\imath+1)(j-1)k} \\
&\quad + [MIJ]_{(\imath+1)(j+1)k}\vec{H}_{(i+1)(j+1)k} \\
&\quad + [MIK]_{(\imath-1)j(k-1)}\vec{H}_{(\imath-1)j(k-1)} \\
&\quad + [MIK]_{(\imath-1)j(k+1)}\vec{H}_{(\imath-1)j(k+1)} \\
&\quad + [MIK]_{(i+1)j(k-1)}\vec{H}_{(i+1)j(k-1)} \\
&\quad + [MIK]_{(\imath+1)j(k+1)}\vec{H}_{(\imath+1)j(k+1)} \\
&\quad + [MJK]_{i(j-1)(k-1)}\vec{H}_{\imath(j-1)(k-1)} \\
&\quad + [MJK]_{\imath(j-1)(k+1)}\vec{H}_{\imath(j-1)(k+1)} \\
&\quad + [MJK]_{\imath(j+1)(k-1)}\vec{H}_{\imath(j+1)(k-1)} \\
&\quad + [MJK]_{\imath(j+1)(k+1)}\vec{H}_{\imath(j+1)(k+1)} = 0 \qquad (3)
\end{aligned}$$

in which

$$\vec{H} = \begin{bmatrix} H_x \\ H_y \\ H_z \end{bmatrix} \quad [M] = \begin{bmatrix} M_x & 0 & 0 \\ 0 & M_y & 0 \\ 0 & 0 & M_z \end{bmatrix}$$

$$[MI] = \begin{bmatrix} 0 & 0 & 0 \\ 0 & M_y & 0 \\ 0 & 0 & M_z \end{bmatrix} \quad [MJ] = \begin{bmatrix} M_x & 0 & 0 \\ 0 & 0 & 0 \\ 0 & 0 & M_z \end{bmatrix}$$

$$[MK] = \begin{bmatrix} M_x & 0 & 0 \\ 0 & M_y & 0 \\ 0 & 0 & 0 \end{bmatrix} \quad [MIJ] = \begin{bmatrix} 0 & M_y & 0 \\ M_x & 0 & 0 \\ 0 & 0 & 0 \end{bmatrix}$$

$$[MIK] = \begin{bmatrix} 0 & 0 & M_z \\ 0 & 0 & 0 \\ M_x & 0 & 0 \end{bmatrix} \quad [MJK] = \begin{bmatrix} 0 & 0 & 0 \\ 0 & 0 & M_z \\ 0 & M_y & 0 \end{bmatrix}.$$

Coefficients M_x, M_y, and M_z are related to the previously defined coefficients CE, CH, RCE, RCH, and $k_0 = \omega\sqrt{\mu_0\varepsilon_0}$. One should notice the symmetry of (3) with respect to the principal axis.

Next, the *cells* are concentrated symmetrically by applying magnetic flux conservation relation (1d). This is performed by deriving two relations, (4a) and (4b), from the magnetic flux conservation between the condensed *cell* ijk (referred to as the reference *cell*) and its six neighboring *cells* along the principal axis. More precisely, *cells* with subscripts $(i-1)jk$, $i(j-1)k$, and $ij(k-1)$ are considered with the backward discretization

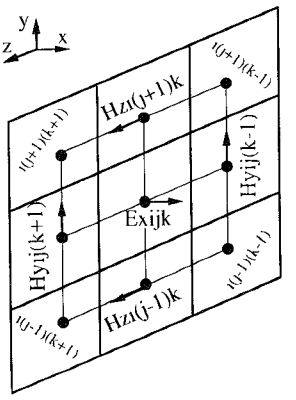

Fig. 2. Discretization scheme for E_x field component at discretepoint $\imath jk$.

whereas *cells* with subscripts $(i+1)jk$, $\imath(j+1)k$, and $ij(k+1)$ are taken into account with the forward discretization. The differential volume considered to apply the flux conservation is presented in Fig. 3, only for $H_{y\imath jk}$ field component,

$$\begin{aligned}
&[CH_{x(i+1)jk}H_{x(i+1)jk} - CH_{x\imath jk}H_{x\imath jk}] \\
&\quad + [CH_{yi(j+1)k}H_{yi(j+1)k} - CH_{y\imath jk}H_{y\imath jk}] \\
&\quad + [CH_{z\imath j(k+1)}H_{zij(k+1)} - CH_{z\imath jk}H_{z\imath jk}] = 0 \qquad (4a) \\
&[CH_{x\imath jk}H_{x\imath jk} - CH_{x(i-1)jk}H_{x(\imath-1)jk}] \\
&\quad + [CH_{y\imath jk}H_{y\imath jk} - CH_{y\imath(j-1)k}H_{y\imath(j-1)k}] \\
&\quad + [CH_{z\imath jk}H_{z\imath jk} - CH_{z\imath j(k-1)}H_{z\imath j(k-1)}] = 0. \qquad (4b)
\end{aligned}$$

To optimize the number of *cells* involved in conserving the symmetry of this formulation, specific rules are followed according to (4a) and (4b). These rules are related to the choice of the reference *cell*. In the beginning, the reference *cells* $(i-1)jk$ and $(i+1)jk$ are used to eliminate H_z field components in the first line of (3) using (4a) and (4b). Next, the reference *cells* $i(j-1)k$ and $i(j+1)k$ are considered to eliminate H_x field components in the second line of (3). Finally, H_y field components in the third line of (3) are removed by considering the reference *cells* $ij(k-1)$ and $ij(k+1)$. This process leads to a 3D condensed *node* (Fig. 4a) whose characteristic relation is not given here for simplicity. Nevertheless, it should be mentioned that it provides solutions in terms of field components H_x, H_y, H_z. Spurious modes are effectively eliminated under the consideration of the flux conservation relations. This point, which solves for six field components, has not been mentioned in other general formulations [19]. Indeed, the flux conservation relations state that there is no net flux lines arising from any static source in the medium. Generally speaking, these spurious modes arise from the fact that the divergence of field vectors is not taken into account since a vector, mathematically, is completely defined if its curl and divergence are simultaneously satisfied. The flux conservation relations are in fact an integral form of the so-called zero divergence relations commonly used to suppress spurious modes when the differential form of Maxwell's equations are considered. More details are given in [15] with regard to this subject.

For 2D analysis, a simplified formulation is developed in terms of transverse fields H_x and H_y by eliminating H_z field components in the first two lines of (3). The final expression characterizing the 2D condensed *node* (Fig. 4(b)) is obtained

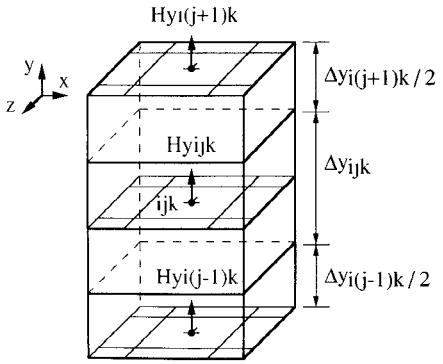

Fig. 3. Discretization scheme for H_y field component considering the flux relation.

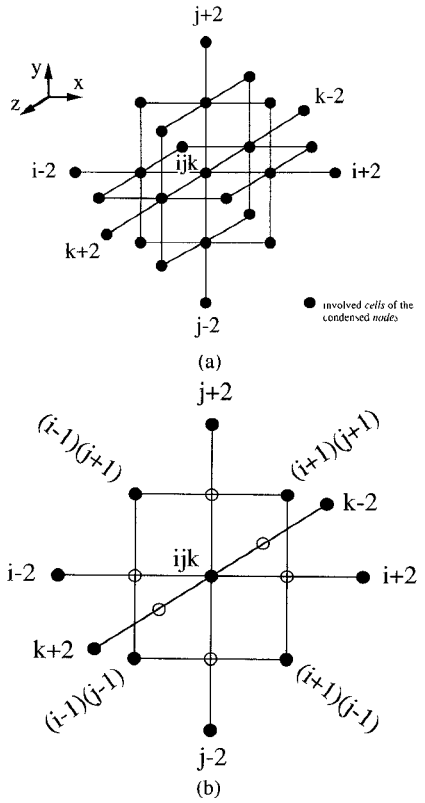

Fig. 4. (a) 3D condensed *node*. (b) 2D condensed *node*.

by using (4a) and (4b) with the reference *cells* $(i-1)jk$, $(i+1)jk$, $i(j-1)k$, and $i(j+1)k$, such as

$$\begin{aligned}&[P]_{ijk}\vec{H}_{ijk} + [P]_{(i-2)jk}\vec{H}_{(i-2)jk} + [P]_{(i+2)jk}\vec{H}_{(i+2)jk}\\&\quad + [P]_{i(j-2)k}\vec{H}_{i(j-2)k} + [P]_{i(j+2)k}\vec{H}_{i(j+2)k}\\&\quad + [P]_{ij(k-2)}\vec{H}_{ij(k-2)} + [P]_{ij(k+2)}\vec{H}_{ij(k+2)}\\&\quad + [Q]_{(i-1)(j-1)k}\vec{H}_{(i-1)(j-1)k}\\&\quad + [Q]_{(i-1)(j+1)k}\vec{H}_{(i-1)(j+1)k}\\&\quad + [Q]_{(i+1)(j-1)k}\vec{H}_{(i+1)(j-1)k}\\&\quad + [Q]_{(i+1)(j+1)k}\vec{H}_{(i+1)(j+1)k} = 0 \qquad (5)\end{aligned}$$

where

$$\vec{H} = \begin{bmatrix} H_x \\ H_y \end{bmatrix} \qquad [P] = \begin{bmatrix} P_x & 0 \\ 0 & P_y \end{bmatrix} \qquad [Q] = \begin{bmatrix} 0 & Q_y \\ Q_x & 0 \end{bmatrix}.$$

The matrix $[P]$ describes field components H_x and H_y, whereas $[Q]$ determines the coupling between these two field components. Coefficients P_x, P_y, Q_x, and Q_y are related to the previously defined coefficients CE, RCE, CH, RCH, and $k_0 = \omega\sqrt{\mu_0\varepsilon_0}$. Similar expressions can be easily deduced for the E field 2D condensed *node*.

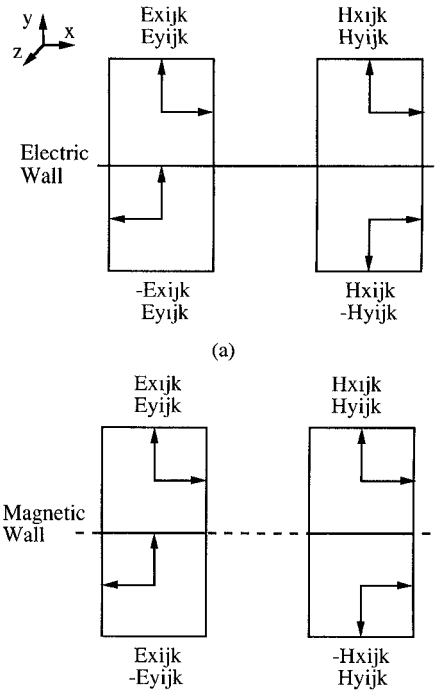

Fig. 5. Image principle applied to *cells* across the boundaries. (a) Electric wall. (b) Magnetic wall.

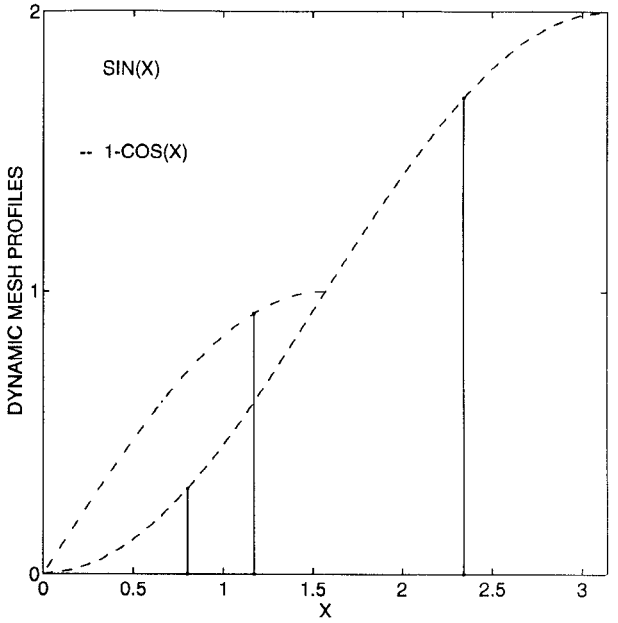

Fig. 6. Dynamic mesh profiles.

III. Boundary Conditions

Considering the field configuration of the condensed *cell* used to form the condensed *node*, an image concept is introduced to model boundary conditions. This concept is derived from the image theory by making an analogy between field components and electric or magnetic sources. Each field component, defined as an electric or a magnetic punc-

TABLE I
DISPERSION CHARACTERISTICS FOR TE_{10} MODE OF A WAVEGUIDE FILLED WITH A LOSSY MEDIUM ($\varepsilon_r = 1.5$, $\tan\delta = 0.1$) AND ERRORS COMPARED TO EXACT VALUES

Normalized Frequency	Normalized Propagation Characteristics		Error Compared to Exact Values [21]		Error Compared to Exact Values from [19]	
k0a	β_z	α_z	$\Delta\beta_z$ (%)	$\Delta\alpha_z$ (%)	$\Delta\beta_z$ (%)	$\Delta\alpha_z$ (%)
0.1	0.025927	- 2.892107	0.014	- 0.036	0.08	- 0.12
0.2	0.076074	- 0.985854	0.063	- 0.065	0.25	- 0.25
0.3	0.646079	- 0.116086	0.066	- 0.065	0.29	- 0.26
0.4	0.943291	- 0.079511	0.018	- 0.016	0.07	0.07
0.5	1.053803	- 0.071173	0.010	- 0.007	0.04	- 0.03
0.6	1.109313	- 0.067612	0.007	- 0.003	0.02	0.02

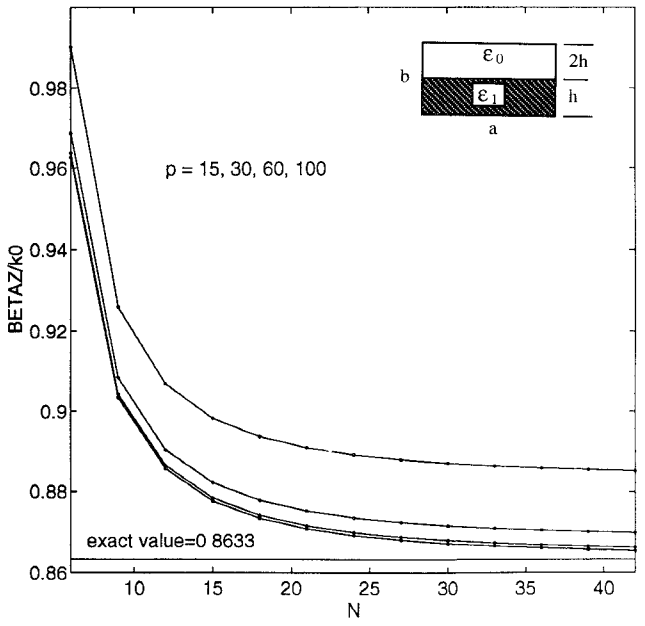

Fig. 7. Convergence behavior of LSE_{y01} mode with $b = 1.016$ cm, $a/b = 2.25$ and $\varepsilon_{r1} = 2.56$.

tual source, is enclosed by the corresponding *cell* cubic box $(\Delta x_{ijk}, \Delta y_{ijk}, \Delta z_{ijk})$. The differential planes $\Delta x_{ijk}\Delta z_{ijk}$ and $\Delta y_{ijk}\Delta z_{ijk}$ act like reflecting planes for the transverse field components at discrete point ijk. Fig. 5 shows how the *cells* across the transverse boundaries are taken into account through the image theory. The boundary *cells* with their images seem to compress the boundaries, thus providing the avoidance of dealing directly with edge singularities. It can be shown that the proposed image principle is somewhat equivalent to Dirichlet and Neumann boundary conditions, and works for any size of the elementary *cell*. If we consider an electric wall, to name an example, the image principle is equivalent to Neumann boundary conditions for tangential H and normal E fields. However, normal H and tangential E fields are subject to Dirichlet boundary conditions by considering the averaging fields on the wall. The dual situation takes place by considering a magnetic wall. Boundary *cells* at right corners are also taken into account through the image principle. It must be noticed that the image principle is only applied at the boundaries; continuity conditions at the interfaces involving different dielectrics have been already considered in the characteristic formulation.

In the following, the 2D analysis in terms of the transverse field components is performed by considering the interaction between all *nodes* defined in the transverse plane. A transverse

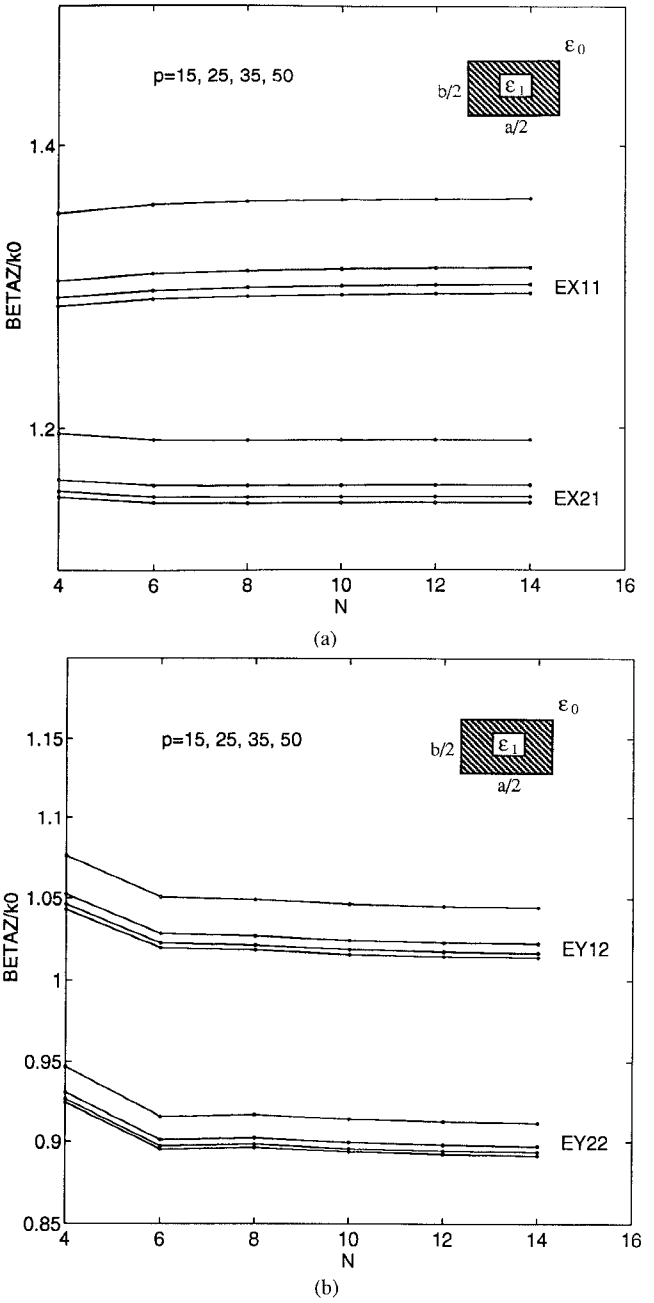

Fig. 8. Convergence behavior of hybrid modes at normalized frequency $V = ak_0\sqrt{\varepsilon_{r1} - \varepsilon_{r0}} = 8$ with $\varepsilon_{r1} = 2.1$. (a) E_{x11} and E_{x21}. (b) E_{y12} and E_{y22}.

plane is defined as a slice of the cross section of a guiding structure with a thickness of Δz in the propagation direction. The whole procedure leads to a standard deterministic eigenvalue problem (6) with a real or complex sparse diagonal matrix for lossless or lossy structures, respectively. Propagation characteristics are obtained by calculating eigenvalues and eigenvectors of (6).

$$([A]) - \lambda I)\vec{H} = 0 \tag{6}$$

where

$\lambda = 2\cosh(2\gamma_z \cdot \Delta z)$	(eigenvalue)
$\gamma_z = \alpha_z + j\beta_z$	(complex propagation constant)
Δz	(mesh size in the propagation direction)
I	(identity matrix).

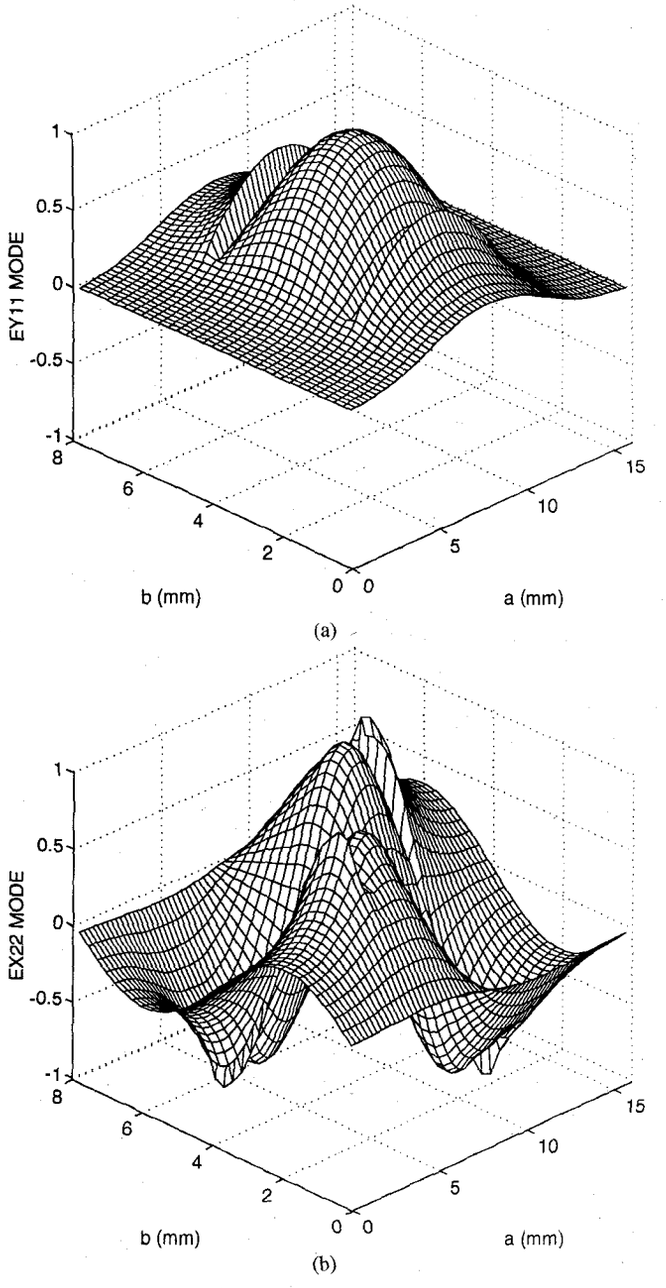

Fig. 9. Field profiles at normalized frequency $V = ak_0\sqrt{\varepsilon_{r1} - \varepsilon_{r0}} = 8$ with $\varepsilon_{r1} = 2.1$. (a) $E_y 11$ mode. (b) $E_x 22$ mode.

The IMSL MATH/LIBRARY package based on EISPACK routines is used to solve the eigenvalue problem. All possible symmetries are exploited to reduce memory size and computation time.

IV. Dynamic Mesh Profiles

Graded mesh is exploited in order to get a better convergence behavior without an excessive discretization. Computation time and memory size can be therefore optimized. This is done by generating discrete points through the use of some profile functions. $\mathrm{SIN}(X)$ and $[1 - \mathrm{COS}(X)]$ (Fig. 6) are chosen as the profile functions providing a smooth variation of mesh size. The range of X is made variable by defining an offset angle XF in order to avoid, if necessary, the saturated zone of the profile functions. In addition, it is

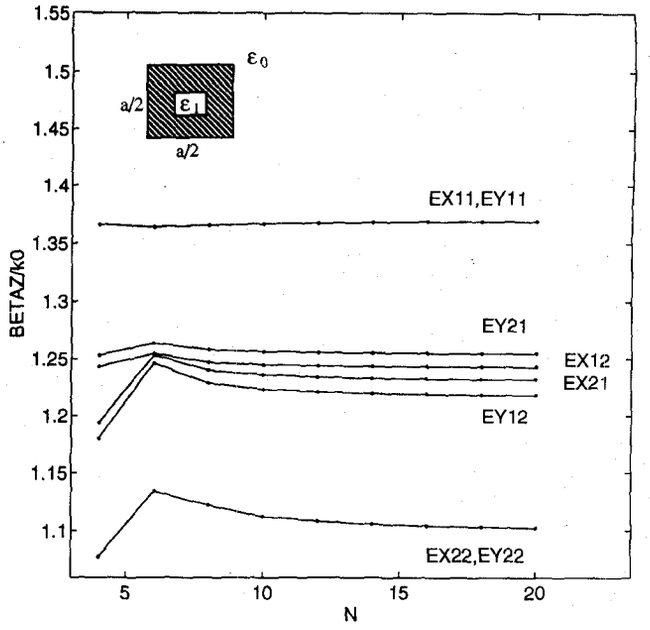

Fig. 10. Convergence of propagation constants of the first eight hybrid modes at normalized frequency $V = ak_0\sqrt{\varepsilon_{r1} - \varepsilon_{r0}} = 8$ with $\varepsilon_{r1} = 2.1$.

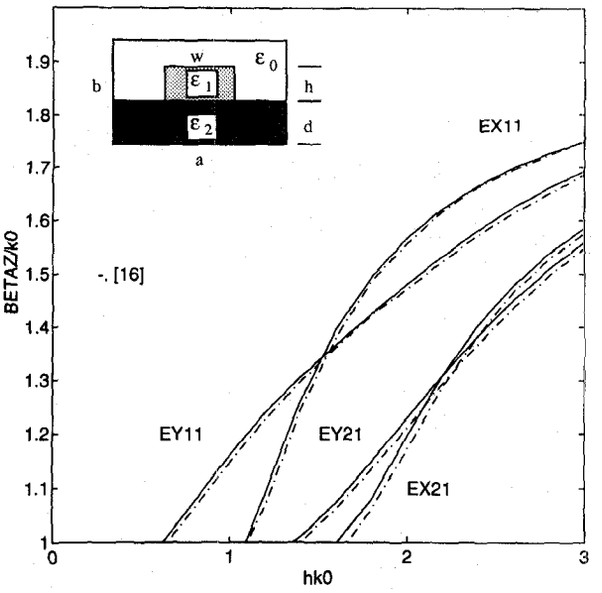

Fig. 11. Dispersion characteristics of an insulated image guide at normalized frequency $V = hk_0$ with $k_0 = \omega\sqrt{\mu_0\varepsilon_0}$, $\varepsilon_{r1} = 3.8$, $\varepsilon_{r2} = 1.5$,$W/h = 2.25$, $d/h = 0.5$, $a/h = 13.5$, $b/h = 8.0$.

observed that a particular value of XF may bring about the optimal convergence. This is important to minimize possible resonance between physical and mesh grid modes [19]. Three types of profiles functions are defined as

$$A \cdot [\mathrm{SCL} \cdot \mathrm{SIN}(X)], \quad 0 \le X \le (\pi/2) - XF \qquad \text{TYPE I}$$

$$A \cdot [1 - \mathrm{SCL} \cdot \mathrm{COS}(X + XF)], \quad 0 \le X \le (\pi/2) - XF \qquad \text{TYPE II}$$

$$A \cdot (1/2) \cdot [1 - \mathrm{SCL} \cdot \mathrm{COS}(X + XF)], \; 0 \le X \le \pi - 2 \cdot XF \qquad \text{TYPE III}$$

where

$$\mathrm{SCL} = \frac{1}{\mathrm{SIN}((\pi/2) - XF)} \quad \text{(scale factor)}$$

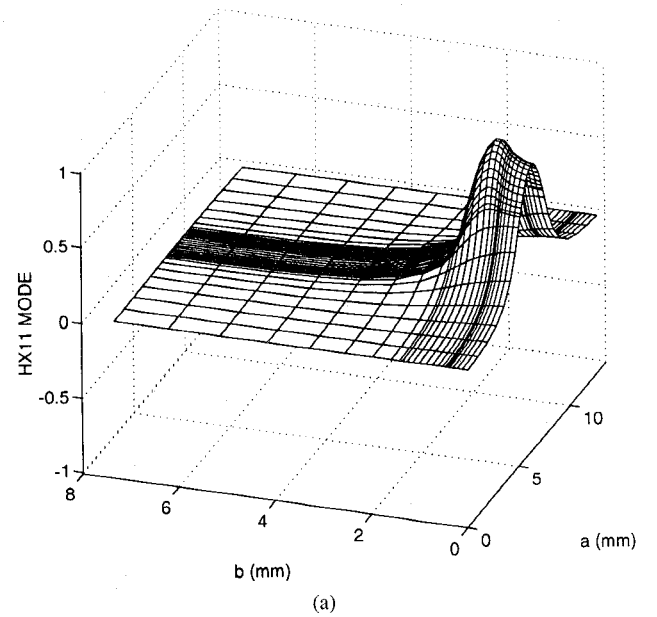

(a)

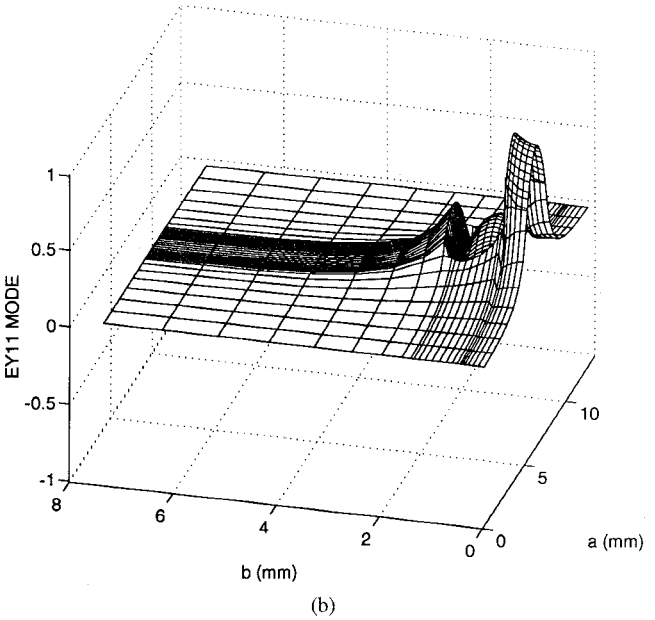

(b)

Fig. 12. Field profiles. (a) H_x11 mode. (b) E_y11 mode.

$$X = i \cdot \frac{(\pi/2) - XF}{N}, \qquad i = 0, 1, \cdots, N \qquad \text{TYPE I, II}$$

$$X = i \cdot \frac{\pi - 2 \cdot XF}{N}, \qquad i = 0, 1, \cdots, N \qquad \text{TYPE III}$$

A: physical dimension to be discretized.
N: number of condensed *cells* required along the physical dimension A.

Quasi equidistant meshes can be generated by choosing a large value for the offset angle XF within the range $[0, \pi/2]$.

V. Numerical Results

A rectangular waveguide of width $= 10a$ and height $= 5a$, filled with a lossy medium, is studied with equidistant meshes. Dispersion characteristics are presented in Table I for the fundamental mode TE_{10} at various normalized frequencies $k_0 a$ where $k_0 = \omega\sqrt{\mu_0 \varepsilon_0}$. The mesh dimensions $(NX, NY) = (40, 20)$ are considered where NX and NY represent the number of condensed *cells* along x- and y-axis, respectively. These results demonstrate the accuracy of this new formulation compared to previous works based on Yee's *cell* [19] and the exact values [21]. The cutoff frequency is located between normalized frequencies 0.2 and 0.3, where a transition from attenuating waves to propagation is observed. The maximum error obtained around the cutoff frequency can be explained by the resonance between physical mode and mesh grid mode [19]. This maximum error, using this formulation over the frequency range of interest is less than 0.07% compared to 0.3% obtained by other formulations [19].

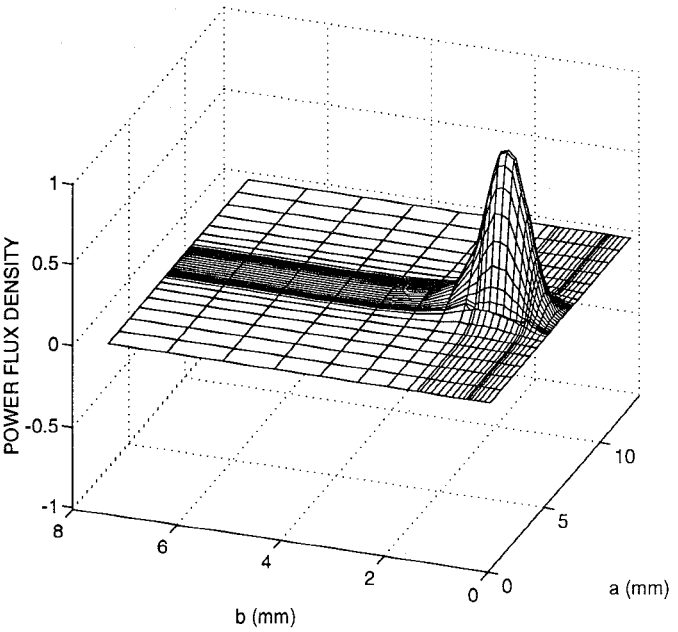

Fig. 13. Power-flux density related to modal fields E_x11 and H_y11.

Results for a partially filled waveguide is presented in Fig. 7, where $N = NX = NY$ and $p = (\lambda/\Delta z)$. A better convergence is achieved as Δz becomes smaller compared to the guided wavelength. This can be explained by the fact that the ideal discretization condition with $\Delta z = 0$ is approached. The results show a good agreement with the exact values [21].

The convergence behavior of the fundamental and higher order modes for a dielectric waveguide is illustrated in Fig. 8. Field profiles of E_y11 and E_x22 are plotted in Fig. 9. It demonstrates loss advantages using a dielectric waveguide since the field is mainly bounded into the dielectric region. Tangential E fields are continuous at the dielectric interfaces in contrast to the discontinuity of normal counterparts. This is consistent with the continuity conditions. Results for a similar dielectric waveguide are shown in Fig. 10 and successfully compared with [18]. The convergence behavior of the first eight hybrid modes $(E_x11, E_x12, E_x21, E_x22, E_y11, E_y12, E_y21, E_y22)$ is shown for $\Delta z = \lambda/50$.

An insulated image guide is also calculated using a different dynamic mesh profile. It is observed that sharp fields at dielectric edges are well determined without a special mesh refinement, resulting in a substantial gain in calculation time and memory size. This is attributed to the use of the condensed *cell* and the central difference scheme. Dispersion characteristics of

hybrid modes E_x11, E_x21, E_y11, and E_y21 are presented in Fig. 11 where a mesh size of $(NX, NY) = (12, 15)$ is used. These results agree well with [16]. The modal fields E_y11 and H_x11 are presented in Fig. 12 at $hk_0 = 1.2$. Tangential H fields vanish on the sidewalls and ohmic losses are then minimized. The modal field E_y11 compares well with [12]. An identical propagation constant is found for modal fields E_x11 and H_y11 at $hk_0 = 1.3$. The related power flux density ($S = E_x11 \times H_y11^*$) is plotted in Fig. 13 showing maximum power around the inner dielectrics.

VI. Conclusion

A new finite-difference frequency-domain formulation that introduces 3D and 2D condensed *nodes* is presented. These condensed *nodes* are derived from condensed *cells* and the integral form of Maxwell's equations. Spurious modes are suppressed by reinforcing the electric and magnetic flux conservation between neighboring *cells*. The image theory is exploited to model boundary conditions. The derived 2D condensed *node* is used to study a variety of waveguiding structures with the deterministic standard eigenvalue solution. Propagation characteristics and modal field profiles are obtained with good accuracy compared to other works. Appropriate dynamic mesh profiles are used to alleviate problems related to the resonance between physical modes and mesh grid modes, while CPU time and memory size are optimized.

References

[1] Z. J. Cendes, "Unlocking the magic of Maxwell's equations," *IEEE Spectrum*, pp. 29–33, Apr. 1989.

[2] K. S. Yee, "Numerical solution of the initial boundary value problem involving Maxwell's equations in isotropic media," *IEEE Trans. Antenn. Propagat.*, vol. AP-14, no. 3, pp. 302–307, May 1966.

[3] A. Taflove and M. E. Brodwin, "Numerical solution of study-state electromagnetic scattering problems using the time-dependent Maxwell's equations," *IEEE Trans. Microwave Theory Tech.*, vol. MTT-23, no. 8, pp. 623–630, Aug. 1975.

[4] D. H. Choi and W. J. R. Hoefer, "The finite-difference time-domain method and its application to eigenvalue problems," *IEEE Trans. Microwave Theory Tech.*, vol. MTT-34, no. 12, pp. 1464–1470, Dec. 1986.

[5] W. K. Gwarek, "Analysis of arbitrarily shaped two dimensional microwave circuits by finite-difference time-domain method," *IEEE Trans. Microwave Theory Tech.*, vol. 36, no. 4, pp. 738–744, Apr. 1988.

[6] D. M. Sheen, S. M. Ali, M. D. Abouzahra, and J. A. Kong, "Application of the three-dimensional finite-difference time-domain method to the analysis of planar microstrip circuits," *IEEE Trans. Microwave Theory Tech.*, vol. 38, no. 7, pp. 849–857, July 1990.

[7] W. Sui, D. A. Christensen, and C. H. Durney, "Extending the two-dimensional FDTD method to hybrid electromagnetic systems with active and passive lumped elements," *IEEE Trans. Microwave Theory Tech.*, vol. 40, no. 4, pp. 724–730, Apr. 1992.

[8] Z. Chen, M. M. Ney, and W. J. R. Hoefer, "A new finite-difference time domain formulation and its equivalent with the TLM condensed node," *IEEE Trans. Microwave Theory Tech.*, vol. 39, no. 12, pp. 2160–2169, Dec. 1991.

[9] D. A. Al-Mukhtar and J. E. Sitch, "Transmission-line matrix method with irregularly graded space," *Proc. Inst. Elec. Eng.*, vol. 128, pt. H, no. 6, pp. 299–305, Dec. 1981.

[10] P. B. Johns, "A symmetrical condensed node for the TLM method," *IEEE Trans. Microwave Theory Tech.*, vol. MTT-35, no. 4, pp. 370–377, Apr. 1987.

[11] H. Jin and R. Vahldieck, "The frequency-domain transmission line matrix method—A new concept," *IEEE Trans. Microwave Theory Tech.*, vol. 40, no. 12, pp. 2207–2218, Dec. 1992.

[12] C. Bulutay and S. Prasad, "Analysis of millimeter waveguides on anisotropic substrates using the three-dimensional transmission-line matrix method," *IEEE Trans. Microwave Theory Tech.*, vol. 41, no. 6/7, pp. 1119–1125, June/July 1993.

[13] A. K. Tiwari, B. Bhat, and R. P. Singh, "Generalized coupled dielectric waveguide and its variants for millimeter-wave applications," *IEEE Trans. Microwave Theory Tech.*, vol. MTT-34, no. 8, pp. 869–875, Aug. 1986.

[14] M. Albani and P. Bernad, "A numerical method based on the discretization of Maxwell's equations in the integral form," *IEEE Trans. Microwave Theory Tech.*, pp. 446–449, Apr. 1974.

[15] T. Weiland, "Three dimensional resonator mode computation by finite difference method," *IEEE Trans. Magn.*, vol. MAG-21, no. 6, pp. 2340–2343, Nov. 1985.

[16] K. Bierwirth, N. Schulz, and F. Arndt, "Finite-difference analysis of rectangular dielectric waveguide structures," *IEEE Trans. Microwave Theory Tech.*, vol. MTT-34, no. 11, pp. 1104–1114, Nov. 1986.

[17] A. Christ and H. L Hartnagel, "Three-dimensional finite-difference method for the analysis of microwave-device embedding," *IEEE Trans. Microwave Theory Tech.*, vol. MTT-35, no. 8, pp. 688–696, Aug. 1987.

[18] N. Schulz, K. Bierwirth, F. Arndt, and U. Köster, "Rigorous finite-difference analysis of coupled channel waveguide with arbitrarily varying index profile," *J. Lightwave Technol.*, vol. 9, no. 10, pp. 1244–1253, Oct. 1991.

[19] S. Haffa, D. Hollmann, and W. Wiesbeck, "The finite-difference method for S-parameter calculation of arbitrary three-dimensional structures," *IEEE Trans. Microwave Theory Tech.*, vol. 40, no. 8, pp. 1602–1610, Aug. 1992.

[20] S. B. Worm and R. Pregla, "Hybrid-mode analysis of arbitrarily shaped planar microwave structures by the method of lines," *IEEE Trans. Microwave Theory Tech.*, vol. MTT-32, no. 2, pp. 191–196, Feb. 1984.

[21] C. A. Balanis, *Advanced Engineering Electromagnetics*. New York: Wiley, 1989.

Messan M. Afande was born in Lomé, Togo, on November 11, 1965. He received the Bac. Ing. degree in electrical engineering in 1989 and the Master degree in power electronics in 1992, both from Université du Québec à Trois-Rivières.

He is currently studying towards the Ph.D. degree at École Polytechnique de Montréal, working on numerical 2D and 3D modeling of various types of waveguiding structures, through the use of the finite difference method in frequency domain.

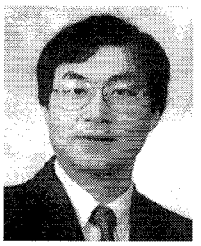

Ke Wu (M'87–SM'92) was born in Jiangsu, China. He received the B.Sc. degree (with distinction) in radio engineering from Nanjing Institute of Technology (now Southeast University), Nanjing, China. He received the D.E.A. degree in electronics and the Ph.D. degree (with distinction) in optics, optoelectronics, and microwave engineering from Institut National Polytechnique de Grenoble (INPG), France.

During the years 1983–1987, he conducted research in the Laboratoire d'Eléctromagnetisme, Microondes et Optoélectronics (LEMO), Grenoble, France. From March 1988 to January 1992 he was a research associate at the University of Victoria, Victoria, BC, Canada, In February 1992, he joined the Département de Génie Électrique et de Génie Informatique at the École Polytechnique de Montréal as an assistant professor. His main research interests include analysis and design of various microwave/millimeter-wave integrated circuits, high-speed interconnects and packaging effects, numerical methods, planar antennas, and superconducting devices. He is also interested in research and design of broadband optoelectronic components and lightwave transmission systems with emphasis on traveling-wave electrooptic modulators, couplers, and switches.

Dr. Wu received an URSI Young Scientist Award in 1987 and, together with two co-authors, the Oliver Lodge Premium from the IEE for an outstanding publication in 1988. He has published more than 100 papers and serves on editorial or review boards of various technical journals.

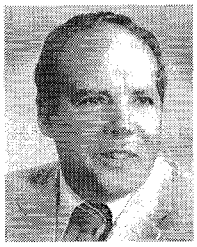

Marcel Giroux is a professor of electrical engineering with the Department of Génie Électrique et Génie Informatique at École Polytechnique de Montréal, from which he graduated in 1959. His primary interest is high-power microwave engineering related to the design and development of energy applicators. He is the Director of the LAIMO Laboratory dedicated to the study of industrial applications of microwave.

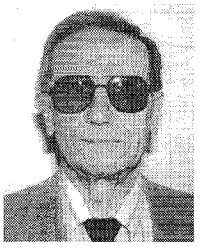

Renato G. Bosisio (M'79–SM'89) received the B.Sc. degree from McGill University, Montreal, Canada, and the M.S.E.E. degree from the University of Florida, Gainesville.

He has been engaged in microwave research and development work with various firms: Marconi and Varian in Canada, Sperry in the USA, and English Electric in England. He is presently Head of Poly-GRAMES, a university microwave research group at École Polytechnique de Montréal, Montreal, Canada, where he teaches microwave theory and techniques. He is actively engaged in six-port technology, dielectric measurements, and computer-aided testing and design of active and passive microwave devices in M(H)MIC.